Journal Homepage: https://dergipark.org.tr/tr/pub/isibted

Isı Bilimi ve Tekniği Dergisi

Archive: https://tibtd.org.tr/dergi

Thermal performance of an evacuated tube solar air heater inserted with copper tubes

A.Veerakumar[1*], T.Karthickmunisamy[1], R.Venkatramanan[2], S.Vijayan[1], R.Parthiban[3] S.Ram Kumar [4], K.Karthi[5],V.Hari Ganesh[6]

[1]Department of Mechanical Engineering, Coimbatore Institute of Engineering and Technology, Coimbatore, 641109, Tamilnadu, India
[2]Department of Mechanical Engineering, Suguna College of Engineering, Coimbatore, 641014, Tamilnadu, India
[3]Department of Mechatronics Engineering, Coimbatore Institute of Engineering and Technology, Coimbatore, 641109, Tamilnadu, India
[4]Department of Mechanical Engineering, Hindusthan College of Engineering and Technology Coimbatore, 641032, Tamilnadu, India
[5]Department of Mechanical Engineering, Sri Sai Ranganathan Engineering College, Coimbatore, 641109, Tamilnadu, India
[6]Department of Mechanical Engineering, RVS College of Engineering and Technology, Coimbatore, 641402, Tamilnadu, India

A R T I C L E I N F O

2026, vol. 46, no.1, pp.156-166

doi: 10.47480/isibted.1827768

Research Article
Received: 22 November 2025
Accepted: 09 April 2026

* *Corresponding Author*
e-mail: veerasees@gmail.com

Keywords:
Air heating systems, solar air heater, copper tube, thermal performance, exergy analysis, double-pass design.

ORCID Numbers in author order:
0000-0001-9554-3988
0000-0003-3369-4750
0000-0003-4324-4622
0000-0001-7370-8876
0009-0001-4557-1213
0000-0001-8881-6685
0009-0004-5713-2255
0009-0002-4960-1221

A B S T R A C T

Solar air heaters (SAHs) are essential for sustainable thermal energy applications, yet their efficiency is often limited by poor internal heat transfer and significant thermal losses. Evacuated tube solar air heaters (ETSAHs) offer improved insulation but require internal modifications to enhance convective heat transfer. This study experimentally investigates the thermal and exergetic performance of a novel double pass evacuated tube solar air heater with copper tube (DPETSAHCT). The present work focuses on improving heat transfer performance while limiting the pressure drop in ETSAH systems. Experiments were conducted under outdoor conditions in Coimbatore, India, across mass flow rates ranging from 10 to 50 kg/h. Performance parameters including outlet temperature, heat gain, thermal efficiency, effective efficiency, pressure drop and exergy efficiency were evaluated. The DPETSAH-CT achieved a maximum outlet air temperature of 110.1°C at 10 kg/h. The highest useful heat gain was 663.8 W at 50 kg/h. Thermal efficiency increased with flow rate, peaking at 40.1%. The system exhibited an effective efficiency of 39.2% and a maximum exergy efficiency of 1.21%. The integration of copper tubes as internal flow guides significantly enhances heat transfer while maintaining manageable pressure drops. The DPETSAHCT design presents a viable, energy-efficient solution for medium-temperature air heating applications, contributing to reduced operational costs and environmental impact.

İçine bakır borular yerleştirilmiş vakumlu tüplü güneş enerjili hava ısıtıcısının termal performansı

M A K A L E B İ L G İ S İ

Anahtar Kelimeler:
Hava ısıtma sistemleri, güneş enerjili hava ısıtıcı, bakır boru, termal performans, ekserji analizi, çift geçişli tasarım.

Ö Z E T

Güneş enerjili hava ısıtıcıları (SAH'ler), sürdürülebilir termal enerji uygulamaları için vazgeçilmezdir, ancak verimlilikleri genellikle zayıf iç ısı transferi ve önemli termal kayıplarla sınırlıdır. Vakumlu tüplü güneş enerjili hava ısıtıcıları (ETSAH'ler) daha iyi yalıtım sunar, ancak konvektif ısı transferini artırmak için iç modifikasyonlar gerektirir. Bu çalışma, bakır tüplü yeni bir çift geçişli vakumlu tüplü güneş enerjili hava ısıtıcısının (DPETSAHCT) termal ve ekserji performansını deneysel olarak araştırmaktadır. Mevcut çalışma, ETSAH sistemlerinde basınç düşüşünü sınırlarken ısı transfer performansını iyileştirmeye odaklanmaktadır. Deneyler, Hindistan'ın Coimbatore şehrinde, 10 ila 50 kg/saat arasında değişen kütle akış hızlarında açık hava koşullarında gerçekleştirilmiştir. Çıkış sıcaklığı, ısı kazancı, termal verimlilik, etkin verimlilik, basınç düşüşü ve ekserji verimliliği dahil olmak üzere performans parametreleri değerlendirilmiştir. DPETSAH-CT, 10 kg/saat'te maksimum 110,1°C çıkış hava sıcaklığına ulaşmıştır. En yüksek faydalı ısı kazancı, 50 kg/saat'te 663,8 W olmuştur. Termal verimlilik, akış hızıyla birlikte artarak %40,1'e ulaşmıştır. Sistem %39,2'lik etkili bir verimlilik ve %1,21'lik maksimum ekserji verimliliği sergiledi. İç akış kılavuzları olarak bakır boruların entegrasyonu, yönetilebilir basınç düşüşlerini korurken ısı transferini önemli ölçüde artırır. DPETSAHCT tasarımı, orta sıcaklıktaki hava ısıtma uygulamaları için uygulanabilir, enerji verimli bir çözüm sunarak işletme maliyetlerinin ve çevresel etkinin azaltılmasına katkıda bulunur.

NOMENCLATURE

D_{et}	diameter of the ET (m)
A_{et}	area of ETs (m²)
N_{et}	total number of ET
I	solar radiation (W/m²)
L_{et}	ET's length (m)
ETC	evacuated tube collector
$\dot{m}$	mass flow rate air (kg/h)
CT	copper tube
ΔP	pressure drop (N/m²)
η_{THE}	effective thermal Efficiency (%)
η_{II}	Exergy efficiency (%)
η_{th}	thermal efficiency (%)
DPETSAH	double pass evacuated tube solar air heater

INTRODUCTION

The solar air heaters (SAH) are very crucial in solar thermal systems because they are designed to be efficient in converting solar energy into heat used to warm air. This warm air can be utilized in various ways such as space heating, drying processes and air conditioning. Further, it has also been studied using numerical analysis on the combination of impinging jets and wire mesh simulators to determine the optimization of mesh dimensions that enhances the thermohydraulic performance with an efficiencies of up to 78% (Agarwal, 2024). Such clean and friendly devices mainly comprise of an airflow duct and an absorber plate, a thin sheet of metallic material, that in this case is used to support the heat exchange process (Parsa et al., 2021). New design absorber plates using aluminum cans or semi-circular shapes have proven to be highly efficient and the semi-circular shape in comparison to circular shape is more efficient due to the more turbulence that breaks the laminar sub layer to increase heat exchange (Can et al., 2024).

The roughness of the surface of the plate absorber promotes the turbulence and thermal efficiency in air heaters. By means of such optimizations, the efficiency is maximized through enhancing the convective heat transfer (Nath et al., 2023). In particular, longitudinal or corrugated fins, baffles have been developed in great detail as a way to increase the heat transfer area and consequently, the thermal efficiency of these systems in general (Kabeel et al., 2017). Triangular baffles have considerable thermal enhancements over wedge and rectangular shape (Lahcene et al., 2024). The turbulators are placed strategically to disturb the laminar sub layer under the absorber plate and hence enhancing the level of turbulence hence, the rate of heat transfer between the absorber surface and the air stream (Arunkumar et al., 2020). Integrating the various approaches, including external airflow recirculation together with the artificial roughness has a great potential in maximizing the efficiency of solar air heating collector compared with what individual changes can provide (Amari et al., 2024).

The ability to include fins and baffles on the plate surface of an absorber has been observed to enhance the thermal efficiency of single or dual pass solar air heaters to a great extent (Omar Mohammed Hamdoon, 2020). Introducing fins, the usage and the application of artificial roughness, i.e., transverse ribs or V-shaped shapes on the backside of the absorber plate has a great impact on the rate of heat transfer as it increases the surface area and causes a turbulence (Bhushan and Singh, 2010),(Chaudhari et al., 2023). V-corrugated absorbers, especially counter flow double pass designs may achieve large improvements in the thermal and exergy efficiencies of flat plate designs and further improvements in the fin density can be achieved through an optimized density (El Ferouali et al., 2018). In addition to these geometrical changes, material characteristics of the absorber plate in itself as well as incorporation of advanced materials including those with selective layers are also significant in the optimization of solar absorption and reduction of radiative heat losses (Pachori et al., 2022).

V shaped and offset rib artificial turbulators include the benefits of significant improvement in the heat transfer and the friction factor with a maximum Nusselt number and friction factors recorded at the certain relative offset rib lengths (Boussouar et al., 2024). It has been demonstrated that the strategic positioning and construction of baffles, their height, as well as setting, impact the airflow and turbulence significantly, resulting in a higher rate of heat transfer in SAHs (Abdukarimov et al., 2023). The fins and baffles increase the turbulence of the secondary flow, thus avoiding the emergence of dead zones and improving the overall heat transfer of the absorber surface (Ibragimov et al., 2023). Staggered fin rows below the plate of absorber have the potential to generate a fully developed turbulent flow, which greatly enhances the thermal heat transfer in relation to systems that have a plain absorber (Hachemi, 1995). It has been demonstrated that the centerline perforated sine wave baffles are the most effective in achieving maximum thermohydraulic performance, and that complex geometries have potential in optimizing the heat transfer (Sharma et al., 2024).

In addition to passive techniques, active flow control devices including those that cause the desired obstacle shapes, e.g. half circles have also been considered as potential to improve the thermal performance of SAHs (Mehranfar et al., 2022). It has been announced that grooved surfaces can enhance thermal performance 1.45 times, discrete symmetric arcs with staggered ribs could achieve peak thermo hydraulic performance at certain ratios between pitch and element and between Reynolds and pitch (Khimsuriya et al., 2024). It has been shown by computational methods that addition of Z shaped baffles to the absorber plate with a particular blockage and pitch ratio can substantially increase the effective efficiency within a particular range of Reynolds number (Ghildyal et al., 2024).

The study experimentally investigated evacuated tube collector (ETC) SAH to enhance thermal performance. The results revealed that optimal effective thermal efficiency of 51.21% at flow of 300 kg/h (Karthickmunisamy et al., 2025). Researchers are therefore diligently striving to adjust the roughness parameters so as to maximize the heat transfer rates whilst reducing the punishment of pressure drop levels (Dubey and Prakash, 2023). Experimental set ups and computational fluid dynamics simulators will be the methods through which the performance of the SAH is evaluated (Maulana Ibrahim et al., 2023). Kumar et al. (2021) studied the experimentally and analytically investigates ETC-SAH with inserted baffles, analyzing the parameters like flow rate and baffle length affect its performance for air heating (Veera Kumar et al., 2021a). It has been shown that certain turbulator designs in the form of circular and V type ribs may result in

85% or more improvement in thermal efficiency at a Reynolds number of 11615 (Rajaseenivasan et al., 2015).

Further numerical studies with ANSYS Fluent have focused on improving such aspects of single V shaped ribs as relative roughness pitch, height and attack angle, to achieve optimal values of up to 1.656 of thermal improvement factors (Rasul et al., 2021). Incorporating ribs into SAHs can improve the thermal efficiency by as much as 9% at lower airflow rates, with curved SAHs achieving Nusselt numbers nearly double those of flat configurations (Ahmadkhani et al., 2021). A major issue with solar air heaters is their inadequate thermal efficiency, which is mainly caused by the sluggish transfer of heat from the absorbing plate to the air duct, resulting in significant heat loss to the surroundings (Singh et al., 2023). Effect of dimpled surfaces for heat transfer were tested for tube layouts with elliptical dimpled fins using DW and Al_2O_3/DW nanofluid, improved Nu by 44.56%. Also, friction factor increased 29.18% at Re = 2000, reducing total S_{gen} 37.75% (Pazarlioğlu and Ekiciler, 2024). In an analysis using ANSYS Fluent 2020R2 to examine anti-icing in aerospace. Tests varied jet-to-surface distances, angles, and slot designs. Aspect Ratio of 4 increased Nu by 85.52% versus circular jet, with triple fold increase in pressure drop (Pazarlıoğlu et al., 2025). Efficient cooling systems enable heat distribution in electronics. Heatsinks are preferred for reliability. Studies under laminar regime (1000 ≤ Re ≤ 2000) examined performance of finned heatsinks with ferro Nano fluid. Maximum figure. of merit occurred at Re = 1500 using square fin heatsink without nanofluid, while lowest entropy and highest heat transfer were reported (Kadir, 2000). Ice accumulation on NACA 0015 airfoil was examined, analysing anti-icing by varying piccolo tube positions under jet angles and optimized performance for maximum heat transfer and minimum pressure drop (Pazarlıoğlu et al., 2022).

Most existing studies on evacuated tube solar air heaters (ETSAHs) have focused on conventional models in which the interior surfaces are smooth. Despite the fact that these designs do a good job of capturing sunlight because of vacuum insulation, transferring the heat to the fluid that passes through the tubes is poor. This study introduces a novel double pass evacuated tube solar air heater with copper tube (DPETSAHCT), where copper tubes are inserted internally to guide airflow, enhance turbulence, and improve heat transfer while monitoring pressure drop. The primary objectives are: (i) To experimentally analyze the thermal and exergetic performance of DPETSAHCT across varying flow rates, (ii) To evaluate heat transfer improvement influences the pressure drop characteristics of the system, (iii) To compare results with conventional ETSAH designs and establish the system's commercial potential. This work addresses a critical research gap by integrating internal flow guides in a double pass evacuated tube (ET) configuration, offering a balanced approach to efficiency and pressure loss management.

METHODOLOGY

Experimental setup

The experiments were conducted in Coimbatore, India (11.0168° N, 76.9558° E) under typical subtropical conditions. The setup comprised ETC with 10 borosilicate glass tubes, each 1800 mm long, with an outer diameter of 58 mm and an absorber tube diameter of 47 mm. Copper tubes (CTs) of 16 mm diameter were inserted into each evacuated tube, creating a double pass airflow path (Fig. 1a). The system detained dimensions are shown in Table 1.

Table 1. Dimension of the experimental setup

S.No	Name	Dimension (mm)
1	ET outer diameter	58
2	ET inner diameter	47
3	CT diameter	16
4	ET length	1800

These ETs were composed of two concentric cylinders made of borosilicate glasses. Between these tubes, a vacuum was maintained to minimize heat loss due to convection. A layer of Al-N/Al was used to coat the absorber tube to maximize the absorption of solar radiation. The tubes were joined to a metal frame at a and connected to the top of an aluminum header with a size of 500 mm × 200 mm × 200 mm. This header has two air flow manifolds, insulated with a thermocouple and glass wool to minimize the amount of heat lost. This was done by blowing air through the collector using a suction blower that was connected to Galvanized Iron (GI) pipes with control valves. The schematic view of the experimental setup along with measuring instruments is shown in Fig. 1(b).

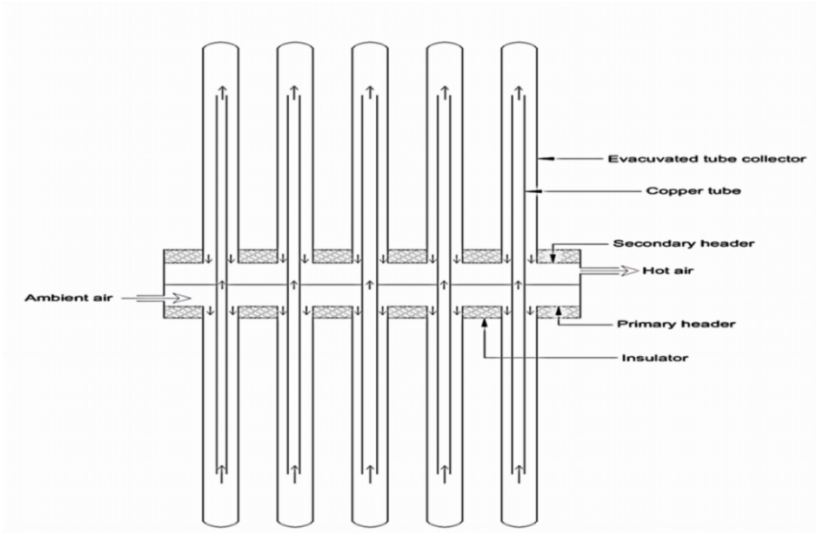

(a)

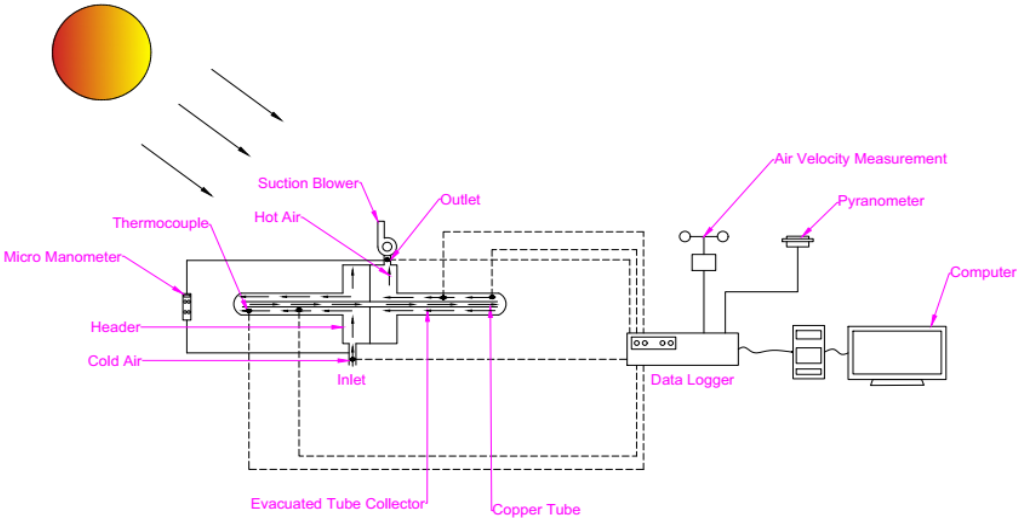

(b)

Fig. 1. (a) Air flow arrangements (b) Schematic view of the DPETSAHCT

The blockage ratio, defined as the cross-sectional area of the copper tube relative to the inner area of the absorber tube, was calculated as approximately 11.6%. This ratio was selected to balance turbulence enhancement and pressure drop.

System operation

The operation configuration of the DPETSAHCT system is illustrated in Fig. 2. The collector has a CT that allows the air to flow in a controlled manner. The ambient air enters the ETC in the square manifold and flows downwards through the CT to the base during the operation. Air is then transported by the evacuated tubes where it is heated by convective heating of the inner absorber surface that is selectively coated. The CT is a thermostat that divides the hot air and the incoming cold air to avoid thermal mixing and enhance heat transfer. The hot air is then passed on to the outlet manifold to be further utilized.

Instrumentation

Temperatures were measured using thermocouples (K-type) (calibration accuracy at ±5 °C) and recorded with a 0.1 °C resolution. The on-site weather station was used to measure outlet air velocity and the solar irradiance. The pressure difference between the inlet and outlet was determined by use of a micromanometer. A first-class pyranometer (accuracy of up to ±2.6%) was used to measure solar irradiance. Fig. 3 presents the photographs of the measurement devices. The uncertainties in measurements of all the input and output variables were also calculated based on the approach in and contrasted with the data provided on the experiment, given in Table 2.

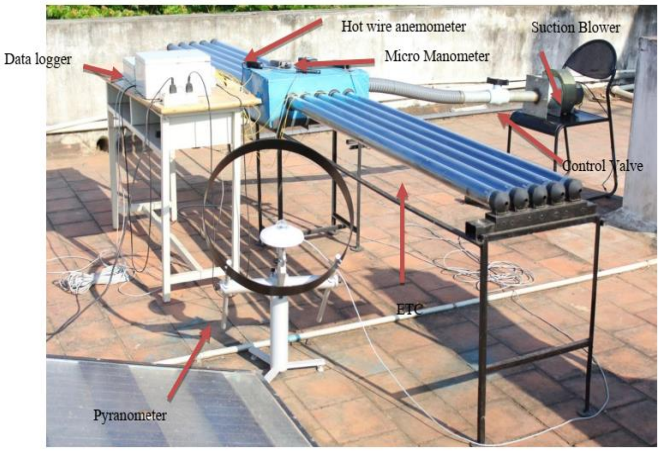

Fig. 2. Pictorial view of the DPETSAHCT

Table 2. Instrument Specifications

S.No	Instrument	Parameter	Accuracy	Standard Uncertainty (u)	Distribution
1.	K-type thermocouple	Temperature	±0.5 °C	0.29 °C	Normal (k=1.73)
2.	Data logger (reading)	Temperature	±0.1 °C	0.06 °C	Normal
3.	Hot-wire anemometer	Air velocity	±2% of reading	0.02 × v	Normal
4.	Pyranometer	Solar irradiance	±2.6% of reading	0.026 × G	Normal
5.	Micromanometer	Pressure drop	±0.2% of reading	0.001 × ΔP	Normal

(a)

(b)

(c)

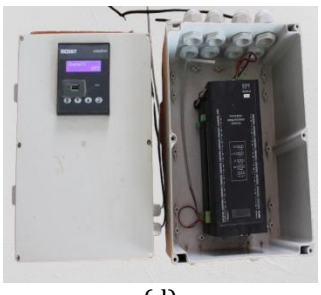

(d)

(e)

Fig. 3. The experimental setup utilized several measuring instruments, (a) Hot-wire anemometer (b) Differential pressure manometer, (c) First-class pyranometer, (d) Data logger, and (e) Weather station with console.

Uncertainty Analysis

Experimental errors and uncertainties may arise from multiple factors, such as the choice and condition of equipment, improper calibration, environmental influences, observational inaccuracies, and errors in measurement readings. Table 3 presents the uncertainties associated with both measured and calculated parameters.

The combined standard uncertainty u_R for a function $R = f(x_1, x_2, \ldots, x_n)$ is calculated as:

$$u_R = \sqrt{\sum_{i=1}^{n} \left(\frac{\partial R}{\partial x_i} \cdot u_{x_i}\right)^2} \quad (1)$$

where u_{x_i} is the standard uncertainty of each measured variable. Uncertainity of the temperature calculated by

$$u_T = \sqrt[2]{\left(u_{thermocouple}^2 + u_{logger}^2\right)} \quad (2)$$

$u_T = \sqrt[2]{0.29^2 + 0.06^2}$=0.296°C ≅ 0.30°C

Uncertainity of the anemometer (typical air velocity of 2.5 m/s) calculated by

$u_v = 0.02 \times 2.5$=0.05m/s (i.e. $\pm 0.05 m/s$) (3)

Uncertainity of solar insolation (pyranometer accuracy ±2.6%) calculated by

u_G =0.026×965=25.09 W/m² (4)

The uncertainty in Heat gain Q_u is:

$$u_{Q_u} = Q_u \sqrt{\left(\frac{u_{\dot{m}}}{\dot{m}}\right)^2 + \left(\frac{u_{C_p}}{C_p}\right)^2 + \left(\frac{u_{\Delta T}}{\Delta T}\right)^2} \quad (5)$$

Where:

- $u_{\dot{m}}/\dot{m} = 1.28/50 = 0.0256$ (2.56%)
- $u_{C_p}/C_p \approx 0.01$ (1%, from property correlations)
- $u_{\Delta T} = \sqrt{u_{T_{out}}^2 + u_{T_{in}}^2} = \sqrt{0.296^2 + 0.296^2} = 0.419$ °C

For a typical condition ($\dot{m} = 50$ kg/h, $\Delta T = 47.5$ °C, $Q_u = 663.8$ W):

$$u_{Q_u} = 663.8 \times \sqrt{\left(0.0256\right)^2 + \left(0.01\right)^2 + \left(\frac{0.419}{47.5}\right)^2}$$

Table 3. Uncertainty/Error for various parameters

S.No	Parameter	Uncertainty
1	Temperature	±0.30 °C
2	Air velocity	±0.05 m/s
3	Solar irradiance	±25.1 W/m²
4	Mass flow rate	±1.28 kg/h
5	Heat gain	±19.2 W
6	Thermal efficiency	±2.18% (abs)
7	Effective efficiency	±2.15% (abs)
8	Pressure drop	±0.1 N/m²

THERMAL PERFORMANCE

The thermal efficiency of the ETC is the ratio of the usable thermal energy acquired to the total solar radiation incident on the collector aperture area (Venkatramanan et al., 2025).

$$\eta_{th} = \frac{Q_u}{A_{et} \times N_{et} \times I} = \frac{\dot{m} C_p \left(T_{1o} - T_{1i}\right)}{A_{et} \times N_{et} \times I} \quad (6)$$

where A_{et} is the aperture area of one ET and it can be determined using the equation (7)

$$A_{et} = 2\, D_{et}\, L_{et} \quad (7)$$

where D_{et} and L_{et} are the diameter of inner tube and length of the ET, N_{et} is the number of ETs, and Q_u is the useful heat gain of outlet air.

In an ETC, the cylindrical absorber surface is exposed to solar radiation over its circumferential area. Due to the transparent outer glass envelope and the evacuated space, solar radiation reaches the absorber surface from the upper hemisphere and is redistributed around the absorber circumference through multiple reflections within the tube. As a result, both the upper and lower halves of the cylindrical absorber surface participates in the heat absorption process.

The factor 2 accounts for the two effective heat absorbing surfaces of the cylindrical tube that contribute to energy transfer to the flowing air inside the tube. This approach has been widely adopted in the literature for evacuated tube solar air heaters to represent the active heat transfer surface interacting with the working fluid.

The solar air heater's performance was assessed by converting the power consumption of the pump into an equivalent thermal energy value. This is assessed by the subsequent relationship (Venkatramanan et al., 2022):

$$\eta_{THE} = \frac{\left(Q_u - \frac{P_m}{C_o}\right)}{A_{te} \times N_{te} \times I} \quad (8)$$

Here C_o = 0.2 (36, 37)

$$P_m = \frac{\dot{m} \Delta P}{\rho} \quad (9)$$

ΔP is the pressure drop between inlet and outlet flow in N/m².

The exergy efficiency of the air heaters is determined using the equation provided below (Veera Kumar et al., 2021c):

$$\eta_{II} = \frac{Ex_{u,p}}{Ex_s} \tag{10}$$

The viable energy gain $(Ex_{u,p})$ is stated as under the postulation of incompressible fluid air and pressure decrease (Warsama and Selimli, 2024).

$$Ex_{u,p} = \dot{m}C_p\left[(T_{1o} - T_{1i}) - T_a\, ln\left(\frac{T_{1o}}{T_{1i}}\right)\right] - \left(\frac{T_a}{T_{1i}}\right)W_p \tag{11}$$

The term $\left(\frac{T_a}{T_{1i}}\right)W_p$ is the exergy destruction due to pressure drop

The net exergy rate provided at the intake of the solar air heater is expressed as

$$Ex_s = SA\left[1 - \frac{4}{3}\left(\frac{T_a}{T_{snu}}\right) + \frac{1}{3}\left(\frac{T_a}{T_{sun}}\right)^4\right] \tag{12}$$

RESULT AND DİSCUSSİON

The variation in the temperature at the air inlet and outlet of the DPETSAHCT was recorded at $\dot{m}$ = 10 kg/h, and the corresponding solar intensity is shown in Fig. 4. It was observed that the outlet temperature was higher at minimum flow rates. Both the outlet and rise in temperature across the collector are directly dependent on the solar insolation. The air outlet temperature increases significantly with an increase in solar insolation, reaching its peak at 1.00 PM, after which it declines as the solar intensity diminishes. A similar pattern was observed for the temperature difference across the collector. At $\dot{m}$ = 10 kg/h, the air passing through the ETC reached a maximum air outlet temperature of 110.1 °C at 1.00 PM. The highest temperature difference across the ETC was 72.6 °C, at I = 965 W/m². On average, the ETC provided the temperature of air is 89.7 °C and a temperature difference of 54.8 °C throughout the day for this flow rate.

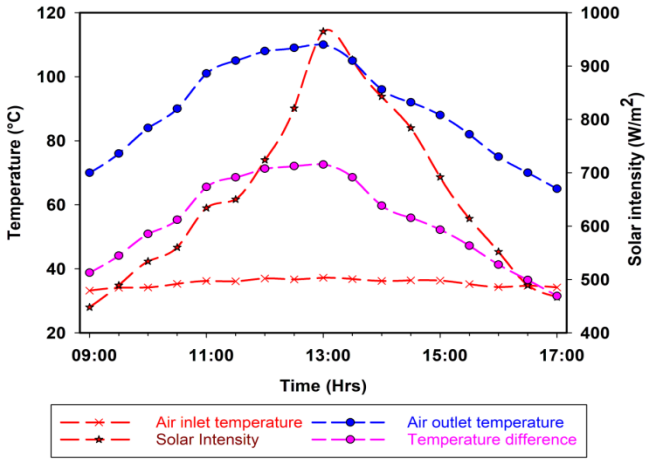

Fig. 4. Temperature of air at inlet, outlet & difference and solar intensity DPETSAHCT at $\dot{m}$ = 10 kg/h

At low mass flow rates (10 kg/h), the air residence time inside the evacuated tube is longer, allowing extended contact with the selectively coated absorber surface. This increases the convective heat transfer time and reduces thermal mixing losses. The Reynolds number is low (1200), indicating laminar to transitional flow, where the thermal boundary layer remains thicker but is continuously disrupted by the presence of the copper tube insert. This disruption prevents the formation of a fully developed laminar sublayer, enhancing conduction through the boundary layer. This trend aligns with Kabeel et al., 2017, who noted that lower flow rates in ETCs yield higher temperature rises due to reduced convective cooling and longer dwell time. Similar findings were reported by Veera Kumar et al., 2021a, where maximum outlet temperatures in baffle-insert ETC systems occurred at minimal flow rates. This trend was consistent for all investigated $\dot{m}$, which ranged from 10 to 50 kg/h.

The variation in the outlet temperature of the DPETSAHCT over time for flow rates between 10 kg/h and 50 kg/h is presented in Fig. 5. As indicated previously, the air outlet temperature is heavily influenced by the solar intensity. It was observed that the outlet temperature increased rapidly with time, reaching its peak between 12.30 PM and 1.00 PM, before starting to decrease. The highest outlet temperatures are achievable between 11.00 AM and 1.00 PM., which coincides with the period of maximum solar intensity. The maximum outlet air temperatures recorded for the respective mass flow rates were as follows. The reason for the enhanced outlet temperature is the increased local heat transfer coefficient, which is a result of induced turbulence. As the flow rate increased, the air temperature outlet decreased because the higher air velocity reduced the contact time for heat transfer. The highest values of air outlet temperature were obtained as 110.1 °C, 103.9 °C, 98.2 °C, 89.7 °C, and 84.9 °C for $\dot{m}$ = 10, 20, 30, 40 and 50 kg/h, respectively, whereas on average temperatures of 89.7 °C, 81.4 °C, 76.5 °C, 70.3 °C, 66.1 °C were noted for the above $\dot{m}$.

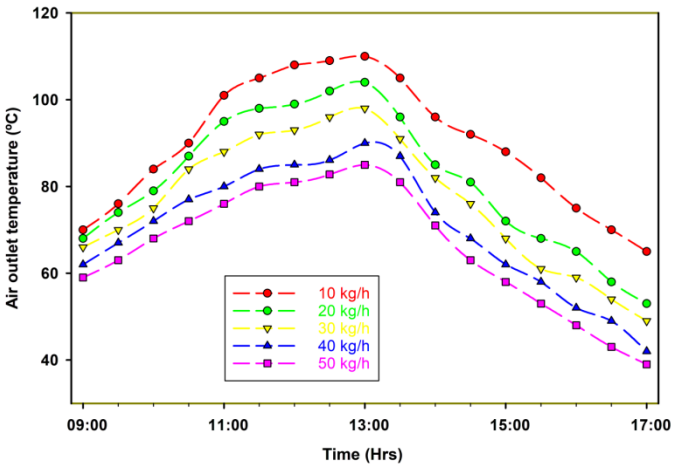

Fig. 5. Air outlet temperature of DPETSAHCT at various $\dot{m}$

As flow rate increases from 10 to 50 kg/h, the Reynolds number rises to 6000, promoting turbulent flow. While turbulence enhances the convective heat transfer coefficient (h), the reduced residence time dominates, limiting the temperature rise. The increased velocity (v) reduces the thermal boundary layer thickness, but the air does not remain in contact with the heated surface long enough to achieve high temperatures. Rajaseenivasan et al., 2015 observed similar behavior in SAHs with turbulators, where outlet temperature decreased by ~25% when flow rate increased by a factor of five, consistent with our findings of a drop from 110.1 °C to 84.9 °C.

Fig. 6 shows the temperature increase across the DPETSAHCT with time for $\dot{m}$ = 10–50 kg/h. Similar trends are seen in the DPETSAHCT temperature rise variations over time, as well as those for the exit air temperatures. As such, the same pattern of increasing temperature rise is found for all the flow rates examined (i.e., 10 to 50 kg/h) from early morning through middle hours; the highest temperature rise occurs during the middle of the day (between 12:30 PM and 1:00 PM) when the amount of solar radiation received by the collector is at its maximum, and the lowest temperature rises are found during the latter portion of the day because of the reduced amounts of solar energy being collected by the collector.

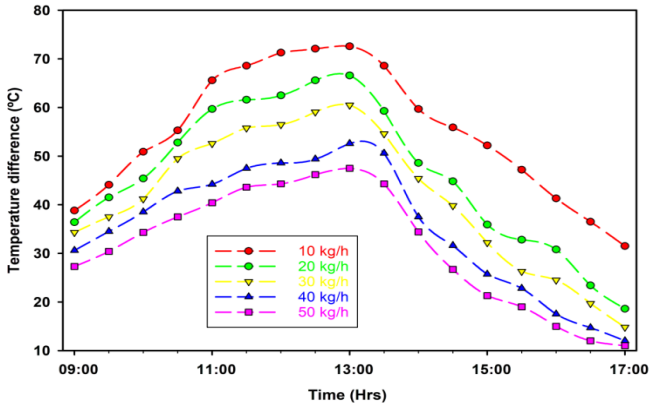

Fig. 6. Temperature rise in DPETSAHCT at different $\dot{m}$

Thus, it can be concluded that there is an extremely good agreement in the thermal responses obtained from DPETSAHCT for all mass flow rates evaluated. The highest temperature rise across the DPETSAHCT is recorded as 72.4 °C, 66.5 °C, 60.5 °C, 52.6 °C, and 47.5 °C for $\dot{m}$ = 10, 20, 30, 40 and 50 kg/h, respectively.

Fig. 7 shows the average temperature increase across the DPETSAHCT with time for $\dot{m}$ = 10 - 50 kg/h. The average temperature rises experienced throughout the day for $\dot{m}$ = 10, 20, 30, 40 and 50 kg/h are approximately 54.8 °C, 46.2 °C, 41.4 °C, 35.3 °C and 31.4 °C, respectively, and demonstrate that the flow rate of the air affects the heat exchange performance of the collector.

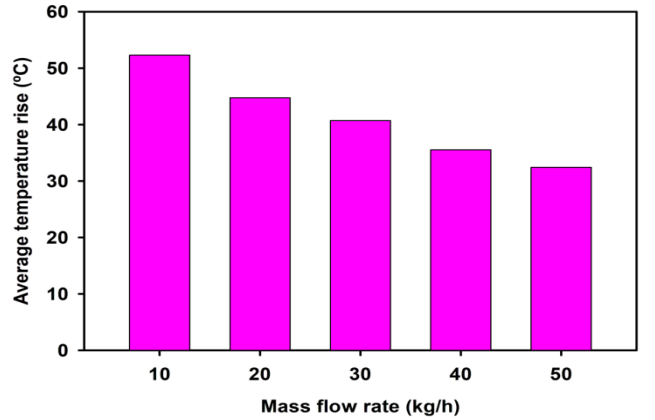

Fig. 7. Average temperature difference in DPETSAH-CT at various $\dot{m}$

All mass flow rates were used to estimate the hourly heat gain of air in the DPETSAHCT. Fig. 8 illustrates the hourly changes in useful heat gain by air for different $\dot{m}$. Heat gain depends on both mass flow rate and temperature difference. Although ΔT decreases at higher flow rates, the increase in $\dot{m}$ is more significant. The copper tube insert enhances turbulence, increasing the Nusselt number, thereby raising the convective heat transfer rate. The double pass design further amplifies heat absorption by exposing the air to heated surfaces twice. Chaudhari et al., 2023 reported similar trends in rib roughened SAHs, where heat gain increased with flow rate despite falling temperature differences, due to enhanced turbulence.

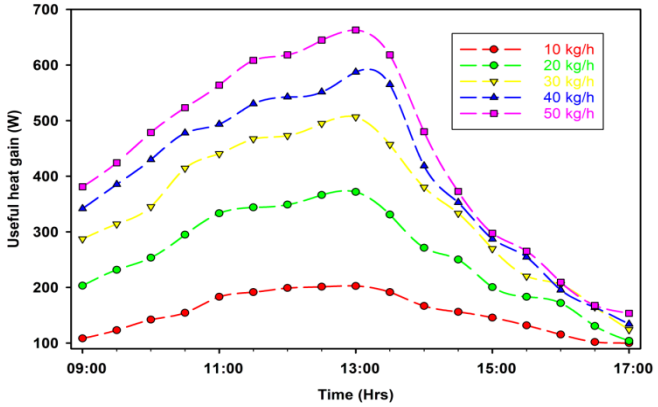

Fig. 8. Heat gain by air in DPETSAHCT at various $\dot{m}$

This variation in heat gain has a similar trend to the temperature difference across the collector because the heat gain is directly proportional to the rise in the temperature of the working fluid. The heat gain increased in the morning hours with a peak of 663.8 W at 1:00 PM at $\dot{m}$ = 50 kg/h an hour, which corresponds to the highest time of solar radiation. After this period, the decrease in the heat gain was slow because of the decrease in incident solar radiation. The mean heat gain of the day was approximately 439.4 W for the same rate of mass flow, which implied constant energy absorption and transfer properties during steady-state operation.

Fig. 9 illustrates the thermal efficiency (TE) of the DPETSAHCT system versus time under the condition $\dot{m}$ = 50 kg/h. Fig. 9 reveals that the TE increases with an increase in the air flow rate. There was a sudden increase in efficiency up to approximately 1:00 PM, after which it started to decrease until 5:00 PM. This movement is similar to the trend in the intensity of solar radiation, which is similar in the period under study. Consequently, the temperature gradient across the collector exhibits a similar trend.

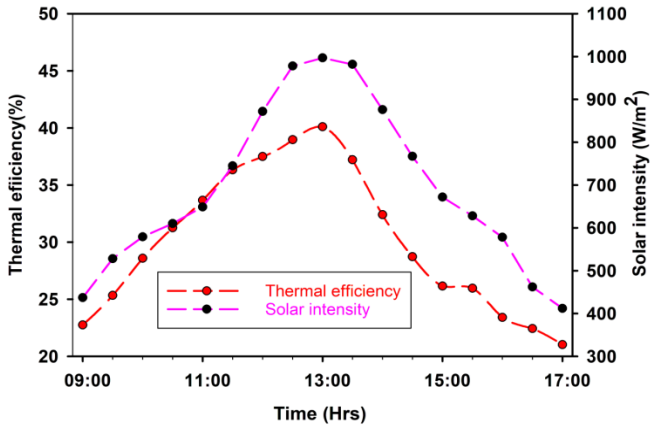

Fig. 9 Solar intensity and thermal efficiency variation of DPETSAHCT at $\dot{m}$ = 50 kg/h

The TE of the DPETSAHCT was investigated with respect to time, and the solar intensity at different $\dot{m}$ is shown in Fig. 10. It was noticed that the instantaneous TE showed a gradual rising tendency with increasing rates of mass flow, which means that the convective heat transfer between the absorber surface and the working fluid was enhanced. There was a

sudden increase in the instant efficiency in the morning hours, which culminated at approximately 1:00 PM to a peak, and then a gradual decrease was observed up to 5:00 PM. This daily cycle was very close to the trend of sun irradiance, which had a similar increase and decrease during such days.

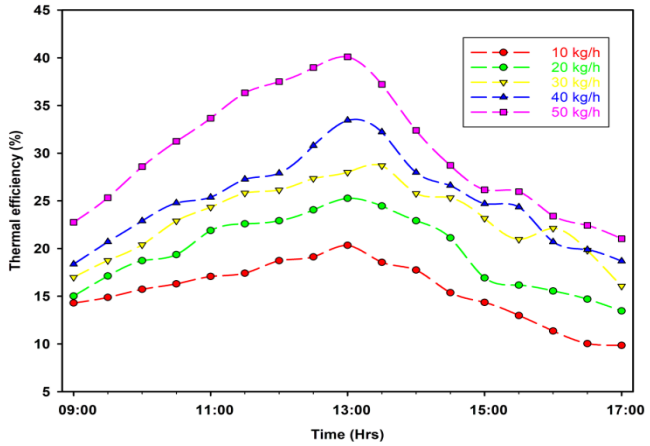

Fig. 10. Thermal efficiency variation of DPETSAHCT at various $\dot{m}$

Thermal efficiency increases because useful heat gain rises with flow rate, while incident solar energy remains constant. The enhanced convective coefficient at higher *Re* reduces the temperature difference between the absorber and air, minimizing thermal losses to the surroundings. The vacuum insulation in evacuated tubes already suppresses convective losses; the added turbulence from the copper tube further optimizes energy extraction. This behavior is consistent with Veera Kumar et al., 2021a who found that baffle insert ETC systems achieved peak efficiencies (52%) at higher flow rates due to improved heat transfer coefficients and reduced relative heat losses.

The difference in solar intensity had a direct impact on the temperature difference across the ETC, such that the behavior of the instantaneous efficiency of the system was controlled. The maximum values of TE at $\dot{m}$ = 10, 20, 30, 40, and 50 kg/h were 20.3%, 25.2%, 27.9%, 30.1%, and 40.1%, respectively. The daily average TE above $\dot{m}$ were 15.2%, 19.3%, 22.1%, 24.5%, and 31.5%, respectively. The highest and lowest thermal efficiencies were 40.1% at $\dot{m}$ = 50 kg/h and 20.3% at $\dot{m}$ = 10 kg/h, respectively, at 1:00 PM.

Fig. 11 shows the pumping power required to operate at various airflow rates and the associated pressure drops in DPETSAHCT. These drops in pressure occurred as a result of constrictions in the flow paths. The airflow rates should be considered to assess the performance of the system.

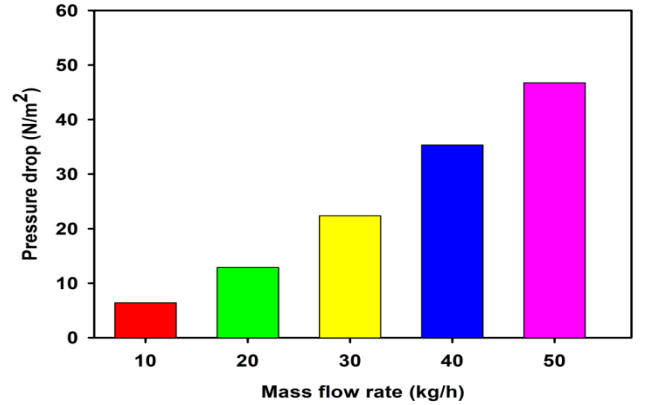

Fig. 11. Pressure drop across the DPETSAHCT at various $\dot{m}$

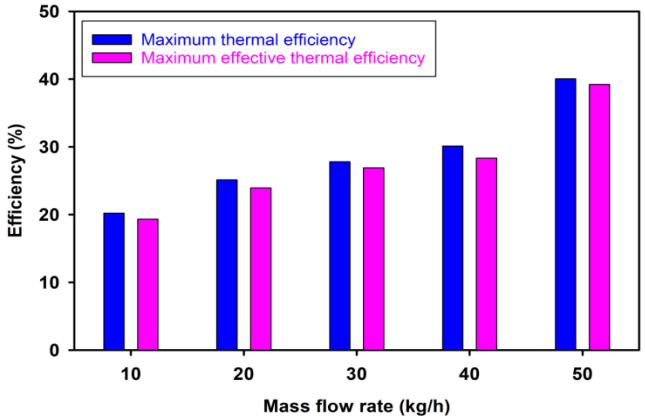

Fig. 12. Maximum thermal and effective efficiencies for various $\dot{m}$

The effective thermal efficiency of the DPETSAHCT plays an important role in determining the optimal airflow rate to achieve optimal system performance (Fig. 12). Above this optimum, the airflow rate increased, and within this range, the pumping power did not increase; however, the temperature increased substantially before the power increased. Moreover, the heat gain was low at low flow rates and the pressure drop increased significantly as the flow of air increased. Both the thermal and effective efficiencies are high in relation to the increased rates of airflow because the more air there is, the better it will be in terms of the distribution of heat. The highest effective thermal efficiency (39.2%) was achieved at $\dot{m}$ = 50 kg/h.

The exergy efficiency is a key measure for evaluating the available energy in a system in relation to its surrounding environment. Fig. 13 illustrates the exergy efficiency of the DPETSAHCT for various $\dot{m}$. The exergy efficiency is strongly affected by the solar irradiance, as shown in the graph. It follows the same trend as solar irradiance, rising with increasing irradiance up to the peak radiation and then decreasing. This increase in exergy efficiency was due to the greater availability of useful exergy. The graph also reveals that, at $\dot{m}$ = 50 kg/h of air, the useful exergy is less than the exergy destruction resulting from the pressure drop.

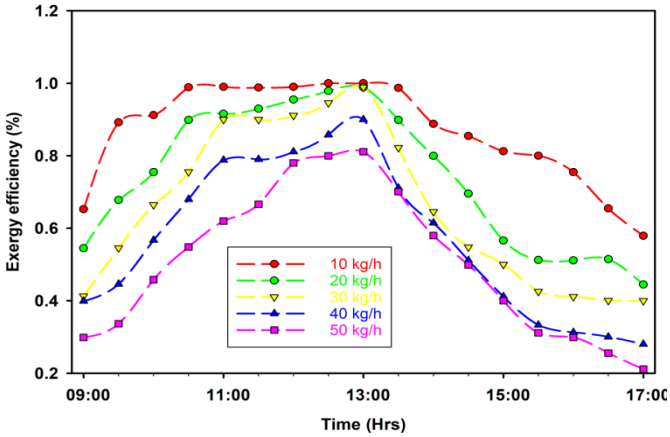

Fig. 13. Variation of exergy efficiency for various $\dot{m}$.

Exergy efficiency declines at higher flow rates because the useful exergy is reduced by increased frictional (pressure drop) losses, which dominate over thermal gains. Although thermal performance improves, the quality of energy (exergy) diminishes due to irreversibilities from fluid friction. El Ferouali et al., 2018 reported similar trends in double-pass SAHs, where exergy efficiency peaked at low flow rates and decreased as turbulent friction losses escalated.

Fig. 14 shows the variations in both the average and maximum exergy efficiency values for the different $\dot{m}$. The maximum exergy efficiencies observed were 1.21%, 0.98%, 0.91%, 0.89%, and 0.82% for $\dot{m}$ = 10, 20, 30, 40, and 50 kg/h, respectively. The average exergy efficiency of the collector at $\dot{m}$ = 10 kg/h was calculated as 0.89%.

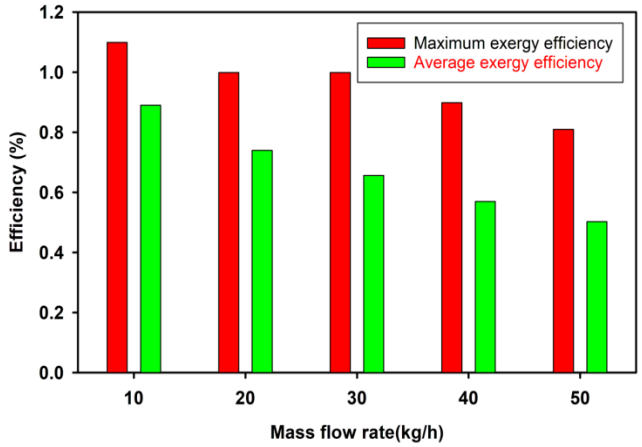

Fig. 14. Effect of $\dot{m}$ on average and maximum exergy efficiency

CONCLUSİON

This experimental investigation focused on DPETSAHCT for air heating purposes at various $\dot{m}$ = 10 to 50 kg/h. The study analyzed the heat gain, outlet temperature, thermal pressure losses, and efficiency.

The key findings are summarized below:

- The DPETSAHCT achieved the highest outlet temperature of 110.1 °C at $\dot{m}$ = 10 kg/h. This shows that the system can produce much higher air temperatures using a sustainable energy source.
- The highest heat gain recorded for DPETSAHCT was 663.8 W at $\dot{m}$ = 50 kg/h. This means that the DPETSAHCT design is able to reduce significantly the normal use of energy and operational expenses in heating of air.
- The DPETSAHCT showed the highest thermal efficiency of 40.1%. This makes it a more energy-efficient thermal system for harnessing solar energy without environmental impacts.
- The highest pressure drop in DPETSAHCT was as 46.8 N/m^2. The highest effective efficiency of 39.2% was attained by DPETSAHCT.
- With the rising energy price and strict emission rules, the energy-saving and optimized designing of the DPETSAHCT. could be an appropriate remedy to the solar air heating services where high outlet temperatures are required as compared to other systems.

The DPETSAHCT configuration improves the compromise between enhanced heat transfer and increased pressure drop in ETSAH systems by integrating copper tubes inside the flow passage, which promote turbulence while maintaining a moderate airflow resistance. Compared to commercial ETSAH units, the DPETSAHCT offers 15–20% higher efficiency at moderate cost increments, making it suitable for industrial air heating and drying applications. Optimization of CT diameter, reflector geometry, and system scaling for higher capacity applications is recommended.

Highlights

- It achieved 110.1°C at a 10 kg/h mass flow rate with sustainable solar heating capability.
- The system recorded 663.8 W of useful heat gain at 50 kg/h, ensuring excellent energy capture performance.
- It peaked at 40.1% thermal efficiency with 39.2% effective efficiency for reliable energy solutions.
- Enhanced convective heat transfer while maintaining manageable pressure drops of 46.8 N/m^2 was achieved.
- Offers 15-20% higher efficiency than commercial units and is ideal for industrial heating applications.

REFERENCES

Abdukarimov, B., Toxirov, M., Jamshidov, O., Mirzayev, S., 2023. Mathematical modelling of heat and hydraulic processes in a solar air heater with a concave air duct absorber. E3S Web of Conferences 452, 04007. https://doi.org/10.1051/e3sconf/202345204007

Agarwal, A., 2024. Optimizing Efficiency of Solar Double-Pass Air Heater through Fluid Combination Approach. E3S Web of Conferences 547, 03026. https://doi.org/10.1051/e3sconf/202454703026

Ahmadkhani, A., Sadeghi, G., Safarzadeh, H., 2021. An in depth evaluation of matrix, external upstream and downstream recycles on a double pass flat plate solar air heater efficacy. Thermal Science and Engineering Progress 21, 100789. https://doi.org/10.1016/j.tsep.2020.100789

Amari, M., Ali, A., Pallathadka, H., AL-Zoubi, O.H., Kaur, H., Kaur, J., Kumar, A., Alzubaidi, L.H., Foladi, A., 2024. Performance study on a new solar air heater for space heating: A numerical and experimental study. AIP Advances 14. https://doi.org/10.1063/5.0243594

Arunkumar, H.S., Vasudeva Karanth, K., Kumar, S., 2020. Review on the design modifications of a solar air heater for improvement in the thermal performance. Sustainable Energy Technologies and Assessments 39, 100685. https://doi.org/10.1016/j.seta.2020.100685

Bhushan, B., Singh, R., 2010. A review on methodology of artificial roughness used in duct of solar air heaters. Energy 35, 202–212. https://doi.org/10.1016/j.energy.2009.09.010

Boussouar, G., Rostane, B., Aliane, K., Ravi, D., Gęca, M.J., Gola, A., 2024. Study of the Thermal Performance of Solar Air Collectors with and without Perforated Baffles. Energies 17, 3812. https://doi.org/10.3390/en17153812

Can, O.F., Celik, N., Ozgen, F., Kistak, C., Taskiran, A., 2024. Experimental and Numerical Analysis of the Solar Collector with Stainless Steel Scourers Added to the Absorber Surface. Applied Sciences 14, 2629. https://doi.org/10.3390/app14062629

Chaudhari, M., Sharma, S.L., Debbarma, A., 2023. Exergetic performance analysis of solar air heater with inverted L-shape ribs as roughness element. Archives of Thermodynamics 241–267. https://doi.org/10.24425/ather.2023.147546

Dubey, M.K., Prakash, O., 2023. Effect of artificial coarseness on the performance of rectangular solar air heater duct: a comparative study. Archives of Thermodynamics 325–358. https://doi.org/10.24425/ather.2023.147549

El Ferouali, H., Zoukit, A., Salhi, I., El Kilali, T., Doubabi, S., Abdenouri, N., 2018. Thermal efficiency and exergy enhancement of solar air heaters, comparative study and experimental investigation. Journal of Renewable and Sustainable Energy 10. https://doi.org/10.1063/1.5039306

Ghildyal, A., Bisht, V.S., Bhandari, P., Thapliyal, S., Kaushik, S., Ranakoti, L., Bangari, R.S., Srivastav, A., Kanojia, N., Paul, A.R., 2024. A comparative numerical evaluation of solar air heater performance having W-contoured, taper-contoured and reverse taper-contoured turbulators. Archives of Thermodynamics 189–196. https://doi.org/10.24425/ather.2024.152008

Hachemi, A., 1995. Thermal performance enhancement of solar air heaters, by a fan-blown absorber plate with rectangular fins. International Journal of Energy Research 19, 567–577. https://doi.org/10.1002/er.4440190703

Ibragimov, U.K., Khamraev, S.I., Shomuratova, S.M., Botirov, A.S., Sattorov, A.B., 2023. Review of methods for improving the thermal performance of solar air collectors with flat plates. BIO Web of Conferences 71, 01048. https://doi.org/10.1051/bioconf/20237101048

Kabeel, A.E., Hamed, M.H., Omara, Z.M., Kandeal, A.W., 2017. Solar air heaters: Design configurations, improvement methods and applications – A detailed review. Renewable and Sustainable Energy Reviews 70, 1189–1206. https://doi.org/10.1016/j.rser.2016.12.021

Kadir, H., 2000. Fe_3O_4/su ile Doldurulmuş Kanatlı Soğutucunun Termodinamik Tersinirlik Açısından Parametrik Analizi, *Düzce Üniversitesi Teknik Bilimler Dergisi*, 1(1),1–10.

Karthickmunisamy, T., Veerakumar, A., Vijayan, S., Venkatramanan, R., 2025. Experimental investigation of an evacuated tube solar air heater with baffles and perforated twisted tapes for air heating applications. Proceedings of the Institution of Mechanical Engineers, Part E: Journal of Process Mechanical Engineering. https://doi.org/10.1177/09544089251368623

Khimsuriya, Y.D., Patel, D.K., Patel, V., Paikra, A.S., Kaushik, L.K., 2024. Heat transfer enhancement in a solar air heater utilizing novel rotating spiral baffles. Journal of Renewable and Sustainable Energy 16. https://doi.org/10.1063/5.0226491

Lahcene, A., Benamara, N., Benguediab, M., Benazza, A., 2024. Efficiency Improvements of Solar Collectors by Turbulence Promoters. Hungarian Journal of Industrial Chemistry 52, 1–9. https://doi.org/10.33927/hjic-2024-13

Maulana Ibrahim, P., Danardono Dwi Prija Tjahjana, D., Yaningsih, I., Rio Prabowo, A., Harsito, C., Enoki, K., Endra Juwana, W., Indro Cahyono, S., 2023. Solar Air Heater Thermal Performance Enhancement using V-Up Continuous Ribs. E3S Web of Conferences 465, 01017. https://doi.org/10.1051/e3sconf/202346501017

Mehranfar, S., Gharehghani, A., Azizi, A., Mahmoudzadeh Andwari, A., Pesyridis, A., Jouhara, H., 2022. Comparative assessment of innovative methods to improve solar chimney power plant efficiency. Sustainable Energy Technologies and Assessments 49, 101807. https://doi.org/10.1016/j.seta.2021.101807

Nath, A., Dabi, M., Teyi, N., 2023. A numerical investigation of a plane solar air heater. E3S Web of Conferences 455, 02001. https://doi.org/10.1051/e3sconf/202345502001

Omar Mohammed Hamdoon, 2020. A Review of Solar Air Heaters: Techniques for Thermal Performance Enhancement. Al-Rafidain Engineering Journal 25, 46–59. https://doi.org/10.33899/rengj.2020.128374.1065

Pachori, H., Mishra, S., Sheorey, T., Choudhary, T., Hanamura, K., 2022. Analytical Study of Energy, Exergy and Thermohydraulic Performance Enhancement of Sustainable Solar Air Heater with C-Shape roughness. https://doi.org/10.21203/rs.3.rs-2245980/v1

Parsa, H., Saffar-Avval, M., Hajmohammadi, M.R., 2021. 3D simulation and parametric optimization of a solar air heater with a novel staggered cuboid baffles. International Journal of Mechanical Sciences 205, 106607. https://doi.org/10.1016/j.ijmecsci.2021.106607

Pazarlioğlu, H.K., Ekiciler, R., 2024. Effect of the Nanofluid Flow And Extended Surfaces On An Abrupt Expansion Tube Regarding Thermodynamic Irreversibility. Heat Transfer Research 55, 49–67. https://doi.org/10.1615/HeatTransRes.2023048288

Pazarlioğlu, H.K., Tepe, A.Ü., Arslan, K., 2022. Optimization of Parameters Affecting Anti-Icing Performance on Wing Leading Edge of Aircraft. European Journal of Science and Technology. https://doi.org/10.31590/ejosat.1062495

Pazarlıoğlu, H.K., Tepe, A.Ü., Arslan, K., 2025. Thermohydraulic performance assessment of new alternative methods for anti-icing application against current application in an aircraft. Proceedings of the Institution of Mechanical Engineers, Part E: Journal of Process Mechanical Engineering 239, 1477–1493. https://doi.org/10.1177/09544089231190182

Rajaseenivasan, T., Srinivasan, S., Srithar, K., 2015. Comprehensive study on solar air heater with circular and V-type turbulators attached on absorber plate. Energy 88, 863–873. https://doi.org/10.1016/j.energy.2015.07.020

Rasul, H.A.M., Hamakhan, I.A., Ibrahim, A.M., 2021. Absorber Type Optimization for Night-Shift Operation of Solar Air Heater. Journal of Engineering Research 9, 1–16. https://doi.org/10.36909/jer.v9iICRIE.11673

Ravichandran, V., Kumar, P.M., Adaikalasamy, V., Gebreyohannes, D.T., 2026. Experimental investigation on solar air heating system using evacuated tube collector with coaxial tube. Scientific Reports 16, 7923. https://doi.org/10.1038/s41598-026-39094-2

Sharma, S., Maithani, R., Randip Kumar Das, 2024. CFD Based Performance Evaluation of Solar Air Heater by

using Centerline Perforated Sine Wave Baffles. Evergreen 11, 862–871. https://doi.org/10.5109/7183368

Singh, S., Suman, S., Mitra, S., Kumar, M., 2023. Optimization of a novel trapezoidal staggered ribs configuration for enhancement of a solar air heater performance using CFD. Environmental Science and Pollution Research 30, 93582–93601. https://doi.org/10.1007/s11356-023-28978-9

Veera Kumar, A., Arjunan, T. V., Seenivasan, D., Venkatramanan, R., Vijayan, S., 2021a. Thermal performance of an evacuated tube solar collector with inserted baffles for air heating applications. Solar Energy 215, 131–143. https://doi.org/10.1016/j.solener.2020.12.037

Veera Kumar, A., Arjunan, T. V., Seenivasan, D., Venkatramanan, R., Vijayan, S., 2021b. Techno-Economic evaluation of an evacuated tube solar air collector with inserted baffles. Proceedings of the Institution of Mechanical Engineers, Part E: Journal of Process Mechanical Engineering 235, 1027–1038. https://doi.org/10.1177/0954408921989847

Veera Kumar, A., Arjunan, T. V., Seenivasan, D., Venkatramanan, R., Vijayan, S., Matheswaran, M.M., 2021c. Influence of twisted tape inserts on energy and exergy performance of an evacuated Tube-based solar air collector. Solar Energy 225, 892–904. https://doi.org/10.1016/j.solener.2021.07.074

Venkatramanan, R., Arjunan, T.V., Seenivasan, D., Veera Kumar, A., 2022. Parametric study of evacuated tube collector solar air heater with inserted baffles on thermal network for low-temperature applications. Journal of Cleaner Production 367, 132941. https://doi.org/10.1016/j.jclepro.2022.132941

Venkatramanan, R., Arjunan, T. V., Seenivasan, D., Kumar, A.V., Selvaraj, V., Matheswaran, M.M., 2025. Energetic and enviro-economic performance of medium scale evacuated tube solar air heating system for industrial applications. Proceedings of the Institution of Mechanical Engineers, Part A: Journal of Power and Energy 239, 388–399. https://doi.org/10.1177/09576509241307457

Warsama, A.I., Selimli, S., 2024. Effect of dust deposition density and particle size on the energetic and exergetic performance of photovoltaic modules: An experimental study. Renewable Energy 226, 120373. https://doi.org/10.1016/j.renene.2024.120373